NASA/TM–2019-220252

Photon Sieve Design and Fabrication for Imaging Characteristics using UAV Flight

Hyun Jung Kim
National Institute of Aerospace, Hampton, Virginia

John Aguillard
Louisiana Tech University, Ruston, Louisiana

Matthew Julian
University of Virginia, Charlottesville, Virginia

Scott Bartram and David Macdonnell
Langley Research Center, Hampton, Virginia

February 2019

NASA STI Program . . . in Profile

Since its founding, NASA has been dedicated to the advancement of aeronautics and space science. The NASA scientific and technical information (STI) program plays a key part in helping NASA maintain this important role.

The NASA STI program operates under the auspices of the Agency Chief Information Officer. It collects, organizes, provides for archiving, and disseminates NASA's STI. The NASA STI program provides access to the NTRS Registered and its public interface, the NASA Technical Reports Server, thus providing one of the largest collections of aeronautical and space science STI in the world. Results are published in both non-NASA channels and by NASA in the NASA STI Report Series, which includes the following report types:

- TECHNICAL PUBLICATION. Reports of completed research or a major significant phase of research that present the results of NASA Programs and include extensive data or theoretical analysis. Includes compilations of significant scientific and technical data and information deemed to be of continuing reference value. NASA counter-part of peer-reviewed formal professional papers but has less stringent limitations on manuscript length and extent of graphic presentations.

- TECHNICAL MEMORANDUM. Scientific and technical findings that are preliminary or of specialized interest, e.g., quick release reports, working papers, and bibliographies that contain minimal annotation. Does not contain extensive analysis.

- CONTRACTOR REPORT. Scientific and technical findings by NASA-sponsored contractors and grantees.

- CONFERENCE PUBLICATION. Collected papers from scientific and technical conferences, symposia, seminars, or other meetings sponsored or co-sponsored by NASA.

- SPECIAL PUBLICATION. Scientific, technical, or historical information from NASA programs, projects, and missions, often concerned with subjects having substantial public interest.

- TECHNICAL TRANSLATION. English-language translations of foreign scientific and technical material pertinent to NASA's mission.

Specialized services also include organizing and publishing research results, distributing specialized research announcements and feeds, providing information desk and personal search support, and enabling data exchange services.

For more information about the NASA STI program, see the following:

- Access the NASA STI program home page at http://www.sti.nasa.gov

- E-mail your question to help@sti.nasa.gov

- Phone the NASA STI Information Desk at 757-864-9658

- Write to:
  NASA STI Information Desk
  Mail Stop 148
  NASA Langley Research Center
  Hampton, VA 23681-2199

NASA/TM–2019-220252

Photon Sieve Design and Fabrication for Imaging Characteristics using UAV Flight

Hyun Jung Kim
National Institute of Aerospace, Hampton, Virginia

John Aguillard
Louisiana Tech University, Ruston, Louisiana

Matthew Julian
University of Virginia, Charlottesville, Virginia

Scott Bartram and David Macdonnell
Langley Research Center, Hampton, Virginia

National Aeronautics and
Space Administration

Langley Research Center
Hampton, Virginia 23681-2199

February 2019

Available from:

NASA STI Program / Mail Stop 148
NASA Langley Research Center
Hampton, VA 23681-2199
Fax: 757-864-6500

Table of Contents

List of Figures

List of Tables

Acronyms

PS – Photon Sieve
IRAD – Internal Research & Development Program
LIDAR – Light Detection and Ranging
FZP – Fresnel Zone Plate
CNF – Cellulose NanoFiber
AMDSB – Advanced Measurements and Data Systems Branch
Cr – Chromium
Fe_2O_3 – Iron Oxide
FL – Focal Length
ASRB – Airworthiness Safety Review Board
CAD – Computer Aided Design
FTOSR – Flight Testing Operational Safety Report
LaRC – Langley Research Center
NASA – National Aeronautics and Space Administration
OWLETS – Ozone Water Land Environmental Transition Study
UAS – Unmanned Aerial System
UASOO – Unmanned Aerial Systems Operations Office
UAV – Unmanned Aerial Vehicle
ATO – Authorization To Operate
RoC – Radius of Curvature
ISO – International Organization for Standardization
DXF – Drawing Exchange Format
CIF – Caltech Intermediate Format
NASA TM – NASA Technical Memorandum
SOA – State-of-the-art
USAF – United States Air Force
OA – Optical Axis
PLA – PolyLactic Acid
EOS – Electro-Optical System
CMOS – Complementary Metal-Oxide Semiconductor
POC – Point-Of-Contact
PVC – PolyVinyl Chloride
fps – frames per seconds

Abstract

The Photon Sieve (PS) team at NASA Langley Research Center (LaRC) began receiving support for the development and characterization of PS devices through the NASA Internal Research & Development Program (IRAD) in 2015. The project involves ascertaining the imaging characteristics of various PS devices. These devices hold the potential to significantly reduce mission costs and improve imaging quality by replacing traditional reflector telescopes.

The photon sieve essentially acts as a lens to diffract light to a concentrated point on the focal plane like a Fresnel Zone Plate (FZP). PS's have the potential to focus light to a very small spot which is not limited by the width of the outermost zone as for the FZP and offers a promising solution for high resolution imaging. In the fields of astronomy, remote sensing, and other applications that require imaging of distant objects both on the ground and in the sky, it is often necessary to perform post-process filtering in order to separate noise signals that arise from multiple scattering events near the collection optic. The PS exhibits a novel filtering technique that rejects the unwanted noise without the need for time consuming post processing of the images.

This project leverages key Langley resources to design, manufacture, and characterize a series of photon sieve specimens. After a prototype was developed and characterized in the Langley ISO5 optical cleanroom and laboratory, outside testing was conducted via the capture of images of the moon by using a telescopic setup.

This next goal of the project is to design and develop a telescope and image capture system as a drone-based instrument payload. The vehicle utilized for the initial demonstration was a NASA hive model 1200 XE-8 research Unmanned Aerial Vehicle (UAV), capable of handling a 20-pound maximum payload with a 25-minute flight time. This NASA Technical Memorandum (NASA-TM) introduces preliminary results obtained using a PS-based imaging system on the UAV. The next version of the telescope structure will be designed around diffractive optical components and commercially available camera electronics to create a lightweight payload.

1. Photon Sieve Project at NASA Langley Research Center

The Photon Sieve (PS) team at NASA Langley Research Center (LaRC) began receiving support for the development and characterization of PS devices through the NASA Internal Research & Development Program (IRAD) in 2015. The project proposed an innovative Light Detection and Ranging (LIDAR) and imaging characteristics concept that could significantly reduce mission costs and improve science/imaging quality by replacing traditional reflector telescopes with PS components.

1.1 Photon Sieve Operating Principle and Characteristics

A PS essentially acts as a lens-like Fresnel Zone Plate (FZP) to diffract light to a concentrated point on the focal plane. However, the PS design differs from a traditional FZP where the FZP rings have been divided up into a large number of pinholes, as shown in Figure 1 (a) and (b) [1]. Typically, the rings of a photon sieve are positioned based on the equation

$$r_n = \sqrt{2n\lambda f + n^2\lambda^2} \qquad \text{[Eq. 1]}$$

where r_n is the radius of the n^{th} ring, λ is the design wavelength, and f is the focal length [2]. Various sizes of PS's can be designed for a targeted wavelength and focal length.

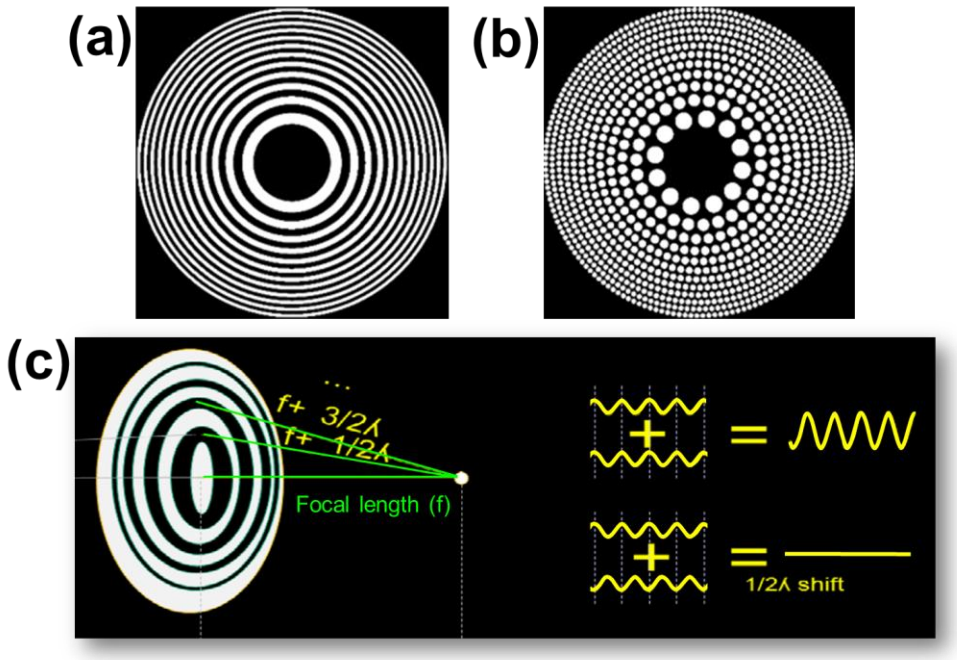

Figure 1. Design of (a) Fresnel Zone Plate (FZP) and (b) Photon Sieve. The center of the PS has progressively larger pinholes versus the outer edge as it is based on a FZP. (c) Schematic diagram of how the PS focuses light. The non-pinhole material (or PS center zone) and neighboring pinhole zones have ½ wavelength differences to the focal point.

Figure 1 (c) shows how the PS focuses light based on the principle of the FZP. The non-pinhole material (dark region) zones and neighboring pinhole zones have a ½ wavelength difference to the focal point. The half-wavelength difference in distance to the focal point cancels the π phase difference of light passing

through the pinholes and thus transferred through the material. The light that destructively interferes with light that passes through the transparent, constructive zones is blocked by dark regions of FZP or PS devices. Thus, the light from the pinhole zones and the non-pinhole zones allows for constructive interference at the focal point and is the entire reason why FZP and PS devices are able to focus. In order to account for this requirement, every second zone (i.e. all odd number zones or all even number zones) is either blocked by an opaque material (amplitude type) or introducing a π phase shift (phase type) to produce constructive interference. The choice of blocking even or odd numbered zones is arbitrary and has no effect on performance.

Photon sieves possess several advantages over other diffractive focusing elements. These include:

(1) The photon sieve shows better focusing ability with suppressed side-lobes than the FZP [1]. The spatial density of pinholes can be modulated ring by ring, which leads to suppression of higher diffracted orders, and thus suppressed side-lobes in the focal plane. This provides photon sieves with inherently greater contrast than zone plates. This improved contrast, combined with superior resolution for a given feature size, should make photon sieves attractive for increased imaging contrast and focusing applications such as various beam-shaping applications [3-6].

(2) Moreover, the PS shows a novel filtering technique by avoiding the unwanted signal without time consuming post processing for imaging applications. In the fields of astronomy, remote sensing, and other applications that require imaging of distant objects both on the ground and in the sky, it is often necessary to perform post-process filtering in order to separate out noise signals that arise from multiple scattering events near the collection optic. For example, in a ground-based LIDAR system, the presence of clouds between the collector and signal altitude can significantly alter the desired science signal by flooding it with noise and other artifacts [7-9]. This post processing is time consuming and often imperfect, and it can be non-trivial to decipher between the true signal and multiple scattering events.

It is envisioned that the PS characteristics will find applications in remote sensing and imaging, with a specific emphasis on LIDAR systems and stellar imaging [11,12].

1.2 Photon Sieve Design and Fabrication

The project uses unique Langley resources to design, manufacture, and characterize a series of photon sieve samples. The Photon Sieve fabrication has been conducted in the ISO5 optical cleanroom facility in building 1247 at LaRC.

The design equations of FZP and PS components are largely the same because a PS is based on a FZP with the zones split into a large number of circular pinholes. One big difference of the PS design is the centers of the sieve pinholes are positioned on the edge of the corresponding Fresnel zones, where only every other ring is counted. This is because the contribution of each pinhole to the focal point intensity is given as a Bessel function of PS [1,12,15]. Based on the Bassel function, the various PS's have been designed for a specific wavelength and focal length using either CIF (script file) or DXF (image file) format design files to specify how to draw the circles in the PS. It is noted that with millions or even billions of holes in a 6-inch diameter PS design, the CIF script file format is more user-friendly and efficient in storing the information to reduce computing time.

The focal length (FL) along with the wavelength, hole ratio, and number of rings is an input parameter for calculating the various geometries of the photon sieve. From the desired magnification of the telescope or image size upon the detector, one needs to determine the required FL and alter the remaining parameters

according to manufacturing limitations (i.e. laser lithography system resolution) and design constraints (i.e. total radius or entire diameter of PS).

Thin films on rigid substrates such as Cr or Fe_2O_3 on soda lime glass substrate are used for traditional or binary / transparent PS fabrications, respectively. For uniform and consistent edge quality for the smallest holes structures (>0.8μm) of the PS, the etching method (wet or dry) and lithography writing heads (10mm head for 1.6μm resolution or 2mm head for 0.8μm resolution) were selected. For space applications, flexible films such as polyimide (Kapton), Mylar, or Cellulose Nanofiber (CNF) film are considered for the merits of light-weight, less-volume, high thermal-stability, low-outgassing, and radiation resistance qualities.

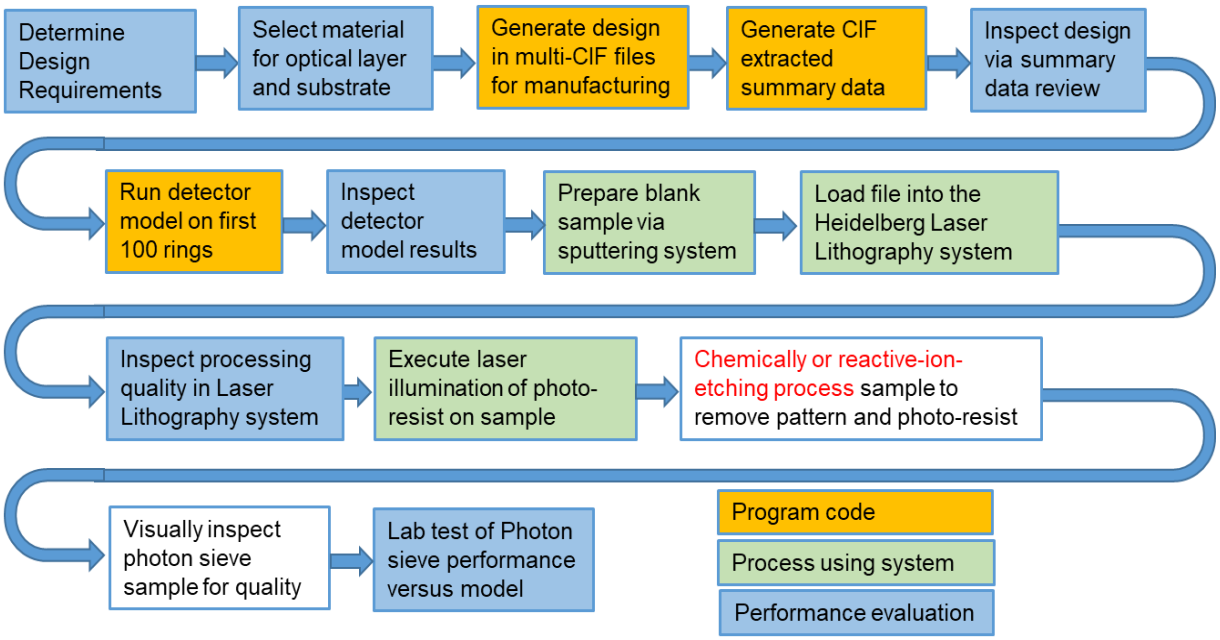

Figure 2. Flow chart of the Photon Sieve manufacturing process at NASA LaRC. The process has been conducted in the NASA Langley ISO5 Optical Cleanroom [13,14]

(1) PS design

The design equations of FZP and PS are largely the same because a PS is based on a FZP with the zones split into a large number of circular pinholes, with one caveat, the centers of the sieve pinholes are positioned on the edge of the corresponding Fresnel zones, with only every other ring counted. Finally, the primary difference between the FZP and PS design is that the photon sieve pinholes can be made larger than the underlying Fresnel zone widths. This is because the contribution of each pinhole to the focal point intensity is given as a Bessel function, as shown by Cao and Jahns [1,12,15]. Specifically, the contribution from each pinhole F is given as

$$F\ \alpha \frac{d}{w} J_1\left(\frac{\pi d}{2w}\right) \qquad \text{[Eq. 2]}$$

where J_1 is the first-order Bessel function of the first kind.

By plotting (2), it can be seen that for various d/w values, the contribution is maximized. Specifically, the function is maximized at $d/w = 1.53, 3.53, 5.53$, and so on. This leads to the relaxed fabrication constraints in photon sieves compared to Fresnel zone plates.

For a typical lens, the resolution (minimum focal spot size) is given by

$$resolution = \frac{\lambda}{2NA} = \frac{\lambda}{2\,sin(\theta)} \quad \text{[Eq. 3]}$$

As we examine the outer edge of the zone plate, is resembles a diffraction grating of grating pitch *2w*, where *w* is the width of the outermost zone. Based on the diffraction grating equation

$$sin(\theta) = \frac{\lambda}{2w} \quad \text{[Eq. 4]}$$

By combining equations (3) and (4), we see that the resolution of the zone plate is equal to the width of its outermost zone, *w*. Furthermore, the resolution of a photon sieve is also governed by the outermost zone width of the underlying zone plate.

Therefore, whereas zone plate resolution is limited by the minimum feature size, photon sieve resolution is not. Hence, for a photon sieve and zone plate with the same focal length, ring number, and diameter, both should focus to the same size point, but the photon sieve will have larger features. Furthermore, for a photon sieve and zone plate with equal minimum feature sizes, the photon sieve will have a tighter focus. Lastly, because the photon sieve is broken up into circular apertures, the apertures can be arranged easily to generate specific wavefront properties which would be difficult to achieve with zone plates.

Based on the Bessel function, the PS designs were generated using either DXF or CIF file formats for fabrication. The manufacturing system used throughout the PS fabrication process was a DWL 66fs laser lithography (Heidelberg Inc.) system. Both DXF and CIF file formats are compatible with the lithography system and are human-readable using various commercial preview and editing programs [13]. Given a 6-inch diameter PS design, with millions or even billions of holes, an optimal method must be developed to streamline the PS design generation and reduce computing time so that it does not take weeks to generate large sieves. For this case, CIF files are clearly more user-friendly and efficient in storing the information due to their script file nature.

The step-by-step process for the generation of both CIF and DXF file formats for 152.5 mm (6 inch) PS fabrication is described in a previous NASA-TM [13].

(2) PS fabrication

The photon sieves are manufactured and evaluated in a cleanroom environment. Microfabrication processes have been adapted to fabricate PS diffractive optical elements similar to semiconductor devices via laser lithography followed by wet or dry etching. Thin films on rigid substrates (i.e. Chromium, Cr or Iron Oxide, Fe_2O_3 on soda lime glass substrate) and flexible polymer films (i.e. Mylar or Kapton) are used for binary PS fabrication. For uniform and consistent edge quality for the smallest holes structures (>0.8μm) of the PS, specific etching methods (either wet or dry) and lithography writing head resolutions (10mm head for 1.6μm resolution or 2mm head for 0.8μm resolution) were selected. The step-by-step process for fabrication of a 6-inch PS is described in NASA-TM [13].

Currently, photon sieve efficiency has been limited to ~1-11%, which has limited its use in several applications such as satellite remote sensing when the reflected light incident on the PS is relatively weak. Alternative binary designs have been investigated in order to increase photon sieve efficiency as well, such as “Fibonacci sieves” and hybrid zone plate/sieve designs [16,17]. However the increases were minimal and resulted in higher side lobes (and thus reduced contrast). Therefore, a new paradigm is needed in photon sieve technology. It is well known that blazed grating zone plates (so-called “Fresnel lenses”) can achieve significantly higher efficiencies than their traditional binary counterparts by up to an order of magnitude. Surprisingly, though, such a concept has not been mentioned or explored for photon sieves. The Langley

team designed and demonstrated a multilevel phase photon sieve, which resulted in a record high efficiency by nearly a factor of three increase as a new paradigm in PS technology. In addition, the multilevel sieve focal plane contained nearly zero side bands, which proves that there need not be a tradeoff between efficiency, resolution, and contrast in the case of photon sieves.

A small size(millimeter diameter) multilevel photon sieve has been successfully demonstrated for the first time as a diffractive optical element with a highest reported efficiency of 49.7%. This is five times higher than any previously reported value [18]. Larger than 25-mm (1-inch) diameter multilevel PS fabrication is currently being performed for imaging applications on a flexible polymer substrate using a grayscale function on the laser lithography system.

(3) ISO5 Optical Cleanroom for PS manufacturing and new material development
The Advanced Measurement and Data Systems Branch (AMDSB) at NASA LaRC has invested in a state-of-the-art (SOA) ISO5 optical cleanroom for research, development, and characterization of optical components. The cleanroom is an environmentally controlled facility. Environmental factors that are controlled include contamination, pressure, temperature, humidity, and static charge. As a class 100 cleanroom, contamination levels are fewer than one hundred particles per cubic foot [19]. This level of control is required for the fabrication and testing of delicate components with demanding fabrication tolerances such as optical components, energy devices and semiconductor devices such as photon sieves and Fresnel zone plates.

Figure 3. Photo of the ISO5 Optical Cleanroom and housed instruments at NASA Langley Research Center

Capabilities afforded with the cleanroom for fabrication of sieves up to 6 inches in diameter on 7 inch substrate include thin film coating, laser-lithography, wet / dry etching, polymer casting, and

characterization of microfabrication for quality control. The instruments are well suited for high-quality PS fabrication. Table 1 shows the instruments and fabrication hardware for PS fabrication in the cleanroom.

Table 1. Current cleanroom instrumentation and fabrication hardware inventory for PS

Categories	Instrument	Manufacture
Patterning	Laser lithography writer	Heidelberg instrument
Characterization	Optical microscopes	Signatone Co
Post-process	Vacuum oven	VWR
Film deposition	RF / DC Sputter	Infovion, Inc
Film deposition	RF / DC Sputter	Nano-Master, Inc
Etching	Wet process benches	
Etching	Relative Ion Etcher	Technics
Pre-process	Spin coater	Laurell
Pre-process	Ozone UV cleaner	Jelight Co, Inc
Pre-process	Ultra-sonic bath	Branson
Pre-process	Hot plate	Fairweather
Pre/ Post	Chemical Hood	ASTEC

1.3 Photon Sieve Imaging Characteristics

After prototypes of PS's were developed in the ISO5 optical cleanroom, a series of indoor and outdoor characterizations were conducted using a United States Air Force (USAF) target and moon images from the telescope setup by using the photon sieves.

1.3.1 Photon Sieve imaging evaluation in the laboratory

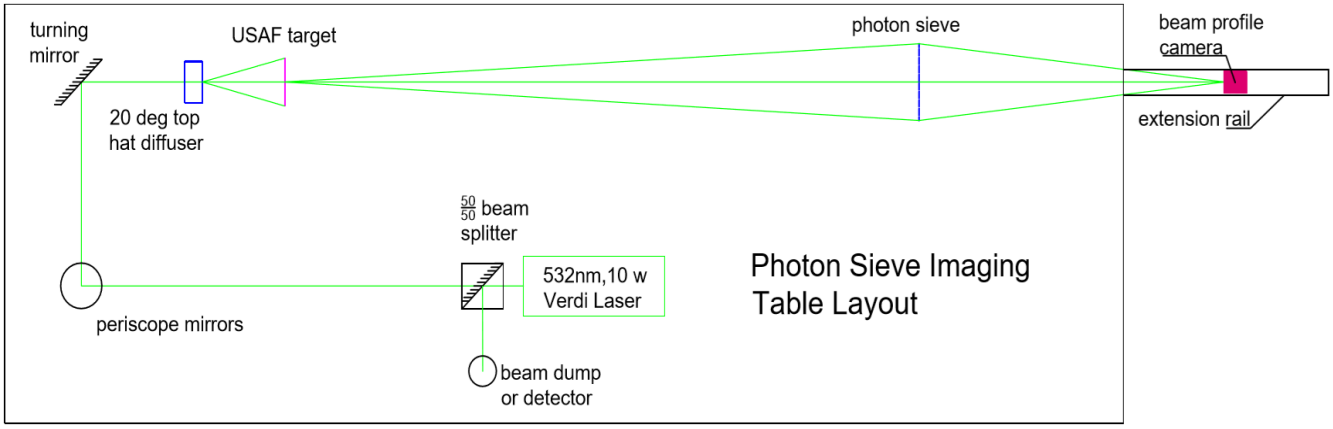

Figure 4. Schematic diagram of the optical table layout for imaging a USAF-1951 target by using a PS and 532nm laser

The figure 4 shows the optical table layout used to image a USAF-1951 (Applied Image Inc., T-22-2) test target by using a PS and laser set up. A 6-inch design of the PS on a 7-inch diameter substrate with a 750-mm focal length (FL) was manufactured for the test. The PS for the United States Air Force (USAF) 1951 imaging was designed to collect the laser light from 3-meters away and reimage it on the camera 500-millimeters past the sieve. The USAF target is patterned on Chromium (Cr) on glass and designed with 3 vertical and 3 horizontal lines in a graduated series. Each set of lines is followed by numbers which give the number of lines/cycles per millimeter.

The light source for imaging was a 10-watt Verdi green laser operating at a 532-nm wavelength. Half of the laser energy was directed to a beam dump through a 50/50 beam splitter as it exited the laser head. This is so that the Verdi system could operate closer to its designed output which makes it more stable. The beam was mirrored to the long axis of the table and through an Edmond Optics 20-degree top hat beam diffuser. The diffuser spread the laser light to illuminate the entire image plane representing the back of the USAF target. Before taking an image, the focus range of the PS was determined. Once a rough focal range was determined, a micrometer was used to make small adjustments in the target position. Images were collected in 0.5 mm apart increments, and the resulting images were analyzed to determine the PS performance depending on the sharpness of each image and the variation of intensity with distance.

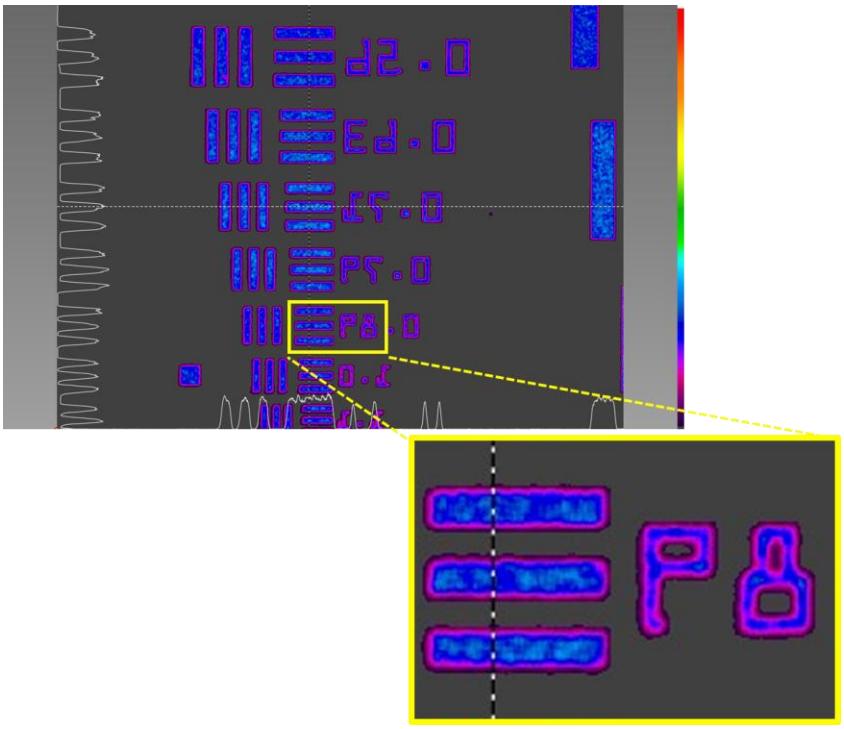

Figure 5. USAF-1951 images through a photon sieve by using the 532nm green laser

Figure 5 shows USAF-1951 images through the photon sieve using a 532-nm green laser. The USAF target produces a very sharp image. The bottom image in Figure 5 shows that .89 lines per mm is clearly resolvable. The numbers were reversed due to a lens effect. The line graph on the left side of the image is a plot of the intensity measured along the dashed line which is visible in the blow-up and extends along the full frame. The colors in the image represent the intensity on the camera's sensor. Based on the rainbow scale on the

right side in Figure 5, the USAF images taken by the PS are well below half of the maximum at this gain and scale since the black and magenta are low energy and red is maximum intensity and white is saturated.

1.3.2 Photon Sieve validation: outside moon imaging

A setup for imaging the moon by using a photon sieve telescope is shown in Figure 6. The telescope is designed to use PS elements with an object distance of infinity and a focal length of 750mm.

The telescope is comprised of a star tracking telescope stand modified to hold a custom optical system. The body of the telescope is a 152.4 mm (6 inch) diameter and 580 mm (23 inch) long PVC Schedule 40 pipe (Genova Products). The pipe has both ends turned so that they are flat and perpendicular to the optical axis (OA). A mount was made to hold the PS centered to the body on the OA by using a 3D printer (Figure 7). The thickness of the outer bezel of the photon sieve holder can be adjusted as shown in Figure 7. The PS holder was printed using white Polylactic Acid (PLA) filament. Multiple versions of the holder have been developed and printed after the first version, exhibiting better tolerances and stability for UAV flights.

The camera end of the telescope has a 3D printed end plate that adapts the 152.4 mm pipe to a 50.8 mm (2 inch) tube system (Thorlabs Inc.). The tube system allows for an adjustable bellows between the camera and the telescope body. The system adapts a narrow band pass filter in order to get a good focus since the chromatic interference without the band pass filter creates a huge blur. A 50.8 mm diameter, 532-nm wavelength band pass filter with a line width of 10μm is mounted in a tube (Thorlabs Inc.) closer to the camera sensor to minimize the clipping.

The camera is mounted on two micrometer stages attached to an extruded aluminum rail so that it can be moved along the OA to allow course adjustment of the focal point. The stages allow for the camera to have a cross axis (*X*) alignment as well as a fine focus (*Z*) adjustment. The camera is a Canon EOS (Electro-Optical System) 80D which has a CMOS (complementary metal-oxide semiconductor) sensor with 24.2 megapixels. This camera has exceptional exposure control as well as real time Wi-Fi downloading of images and video.

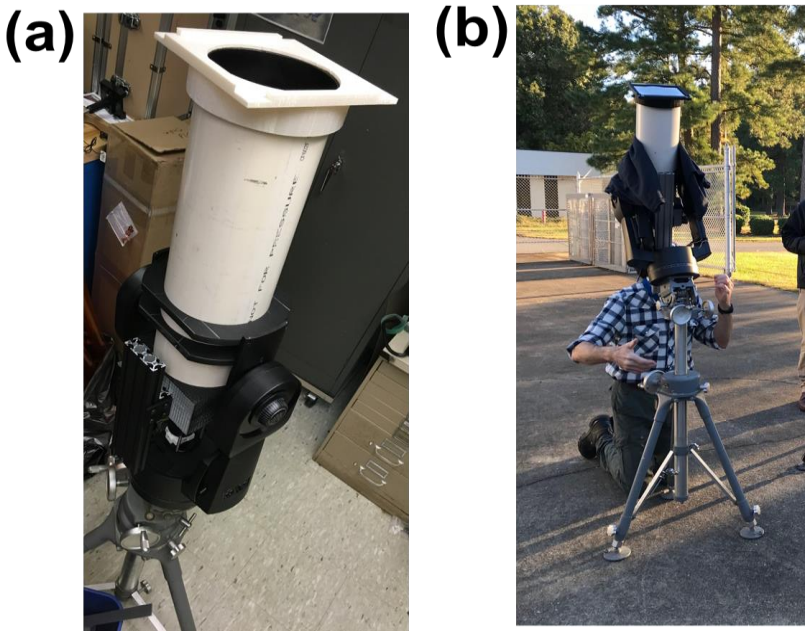

Figure 6. A telescope setup for imaging the moon by using the photon sieve, band pass filter, and camera. The telescope is comprised of a star tracking telescope stand modified to hold a custom optical system.

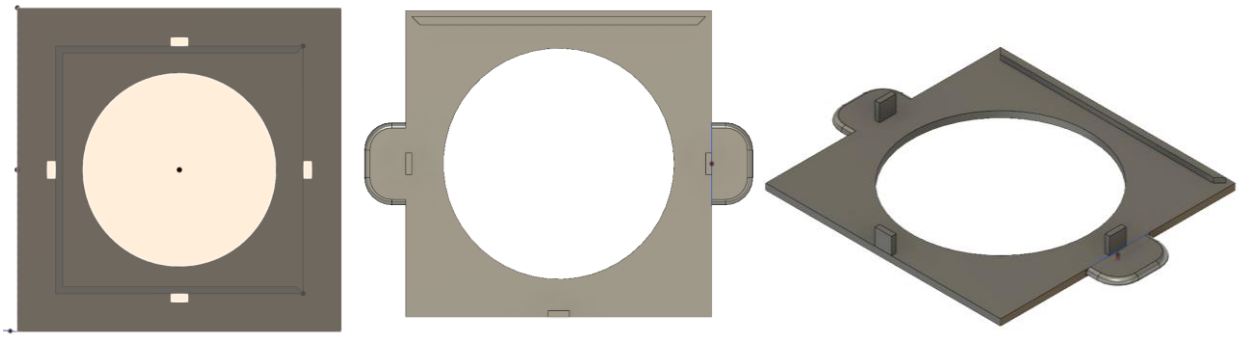

Figure 7. Prototype models of the photon sieve holder for the 3D printing.

Figure 8 (b) show the full moon is well focused and imaged from the telescope setup by using the photon sieve. The image quality is comparable with the image taken by 1.5 meter (61 inch) telescope from Consolidated Lunar Atlas as shown in Figure 8(a). Using a typical lens-camera system such as an iPhone, the moon in obscured by clouds and oversaturates the detector, as seen in Figure 8 (c). From the image comparison between the PS telescope setup (Figure 8 (b)) and iPhone image (Figure 8(c)), the PS has the ability to filter out objects in the near field (clouds) while focusing the far field (moon). In order to prove this concept, we have used a photon sieve with design parameters to image the moon on a cloudy night.

Figure 8. Full moon images taken from (a) Consolidated Lunar Atlas (NASA credit), (b) telescope setup by using the photon sieve, (c) iPhone 7. The results taken from the telescope with PS show the clear Moon focusing and filtering out near field objects such as clouds.

1.3.3 Photon Sieve evaluation: outside checkerboard imaging

For the USAF-1951 target imaging, the PS was designed with different front and rear focal lengths. For the front focus (distance from object of interest / target to photon sieve) 10 meters was selected. The back focus (distance from photon sieve to camera) was set at 0.5 meters. The main body of the imager was made out of 101.6 mm (4 inch) inner diameter, PVC Schedule 40 pipe but with a drain adaptor that would allow a 3D printed PS and a laser mount to be attached (Figure 9). There are 8 class 3A laser diodes from Quartron (model: VLM-532-43-SPA) with a wavelength of 532 nm mounted around the PS on a 114-mm (4.5 inch) radius. Each laser is mounted in a modified 25.4-mm (1-inch) mirror mount (Thorlabs Inc.) and has its own beam expanding telescope. The telescope is comprised of a -25mm lens (Thorlab Inc., model: LC1054-A-ML) and a +50mm lens (Thorlab Inc, model: LA1213-A), assembled in opto-mechanical 50.8-mm (1-

inch) and 225.4-mm (0.5-inch) tube systems. Each telescope needs to be aligned in the laboratory with the telescope expanding the beam to cover the entire target area and the mirror mount adjusted to overlap them all on the focal point of the PS. The lasers are for supplemental illumination of the target along with sunlight.

The camera was attached to a 101.6-mm (4-inch) diameter pipe with a 38.1-mm (1.5-inch) to 76.2-mm (3-inch) diameter PVC adaptor. The 38.1-mm (1.5-inch) side was bored and tapped to mate with a 50.8-mm (2-inch) opto-mechanical tube (Thorlabs Inc., model: SM2). The camera focus was set in the laboratory by first doing a course focus with the PVC adaptor and screwing in place, then a fine adjust was done with the threaded mount and locking ring. The camera was a GoPro, model Hero 6 modified by Backbone Inc. The modification was to remove the stock lens and replace it with a standard "C" lens mount. This mount attached to a "C" mount adaptor (Thorlabs Inc.) and to the 50.8-mm (2-inch) diameter tube.

The Drone Imaging system was taken to a concrete pad adjacent to building 1200 at NASA LaRC and ground tested as shown in Figure 10. The test was done in the afternoon sun without supplemental laser illumination. The imaging system was set up on aluminum rails and pointed across the cement pad at a checker board target. The distance from the PS to the target was measured with a Leica Disto E7500i laser tape measure.

An eyechart on an 210-mm x 297-mm (letter size, 8.5-inch x 11-inch) piece of paper was held in front of the checkerboard, and the second row of the chart is visible in Figure 10. The eyechart was positioned approximately 17 meters in front of the PS and 0.55 meters in front of the checkerboard. The letters on the chart and the checkerboard are both reasonably focused and imaged in the figure. These results show the range of capability of the PS which represents an important result for UAV flight testing using a similar setup. It is noted that since the imaging system uses the SM2 tubes one could also attach a Canon 80D camera, allowing for better image control but at a much higher weight penalty.

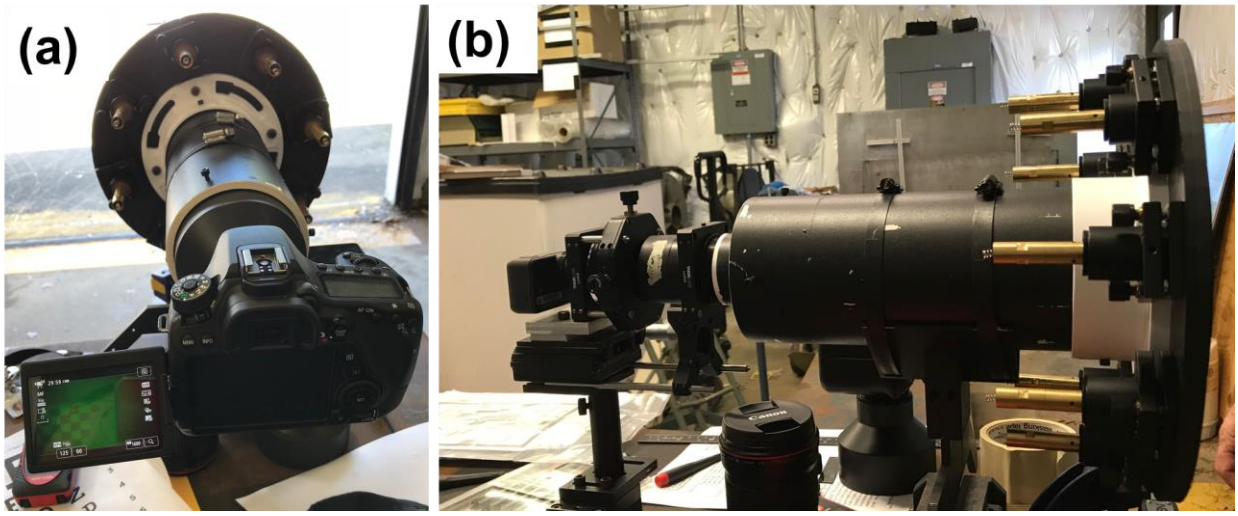

Figure 9. Photos of the setup for the checkboard image test. The main body is made of 101.6 mm (4inch)diameter PVC Schedule 40, photon sieve, laser mount, and cameras, (a) Canon EOS 80D and (b) GoPro Hero 6.

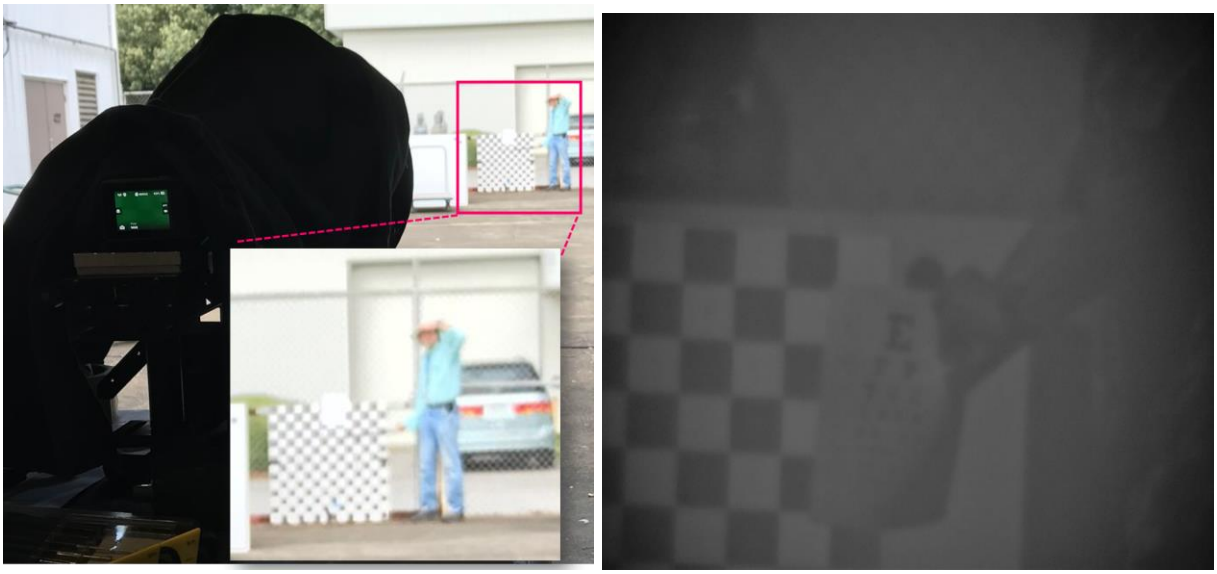

Figure 10. Photos of the checkerboard and eyechart utilized for image testing using a PS. The distance between the setup and the checkerboard and paper are approximately 17 meters and 16.45 meters, respectively. The purpose was to show the range of the photon sieve.

2. UAV flight for characterizing photon sieve imaging

The PS for drone testing required designing a sieve and camera mount light enough to be carried on a drone vehicle. Further, a telescope and image capture system needed to be developed as a drone based instrument. A NASA LaRC Unmanned Aerial Vehicle (UAV, hive model: 1200 XE-8 research) capable of lifting a 9 kilogram (20 pound) maximum payload and exhibiting a 25-minute flight time was used as the vehicle for the flight demonstration. This section introduces some preliminary results of the drone flight using a similar setup as was used for the checkboard imaging tests.

2.1 UAV selection

For the research flight, a UAV with suitable flight characteristics and payload capacity needed to be identified. The original requirements of the project included a 5.4 kilograms (12 pound) lifting capability and a 20 minute run (flight) time.

Figure 11. Selections of the NASA LaRC UAV (left) DJI S1000 (middle) DJI M600 (right) HIVE x8

Three vehicles were considered for the flights. Two DJI drones (an S1000 and a M600) were not used due to their lower weight lifting capabilities. It was decided during a downselect of vehicles that a HIVE x8 (manufactured by Unreal Worx) was best suited for the flight demonstration. The HIVE x8 utilizes a Pixhawk 2.1 flight controller. This flight controller uses ArduPilot, an open source autopilot software, to control the vehicle. ArduPilot is a popular choice among UAV developers due to its powerful data-logging, analysis and simulation tools. This software, when combined with the processors onboard the Pixhawk, should be fully capable of flying the UAV with a new counterbalance. It also can provide the PS team with the ability to program flight patterns for the UAV ahead of time using a desktop computer. Additionally, its advanced data logging and control capabilities could allow it to interface with payload sensors in the future.

2.2 Dummy flight test

After obtaining approval from the LaRC Airworthiness Safety Review Board (ASRB) to proceed with the UAV flight, the PS team began the process of revising the mockup into a usable design. Out of all of the components, the mounting bracket was identified as the single biggest risk of the design, because a failure of the mounting components would likely cause a loss-of-vehicle.

Following an agreement with the ASRB, the PS team was now required to produce a dummy or test payload to begin testing the HIVE with the payload weight without risking the main telescope instrument. By creating a less-expensive, mockup instrument with a similar weight distribution to the real telescope for a drone flight, the team was able to simulate the flight with reduced risk. This flight demonstrated the HIVE x8's ability to lift approximately 7.2~8.2 kilograms (16~18 pounds), which served to satisfy the ASRB's desire for an "incremental build-up" of flights. The first version of the mounting component design shown in Figure 12.

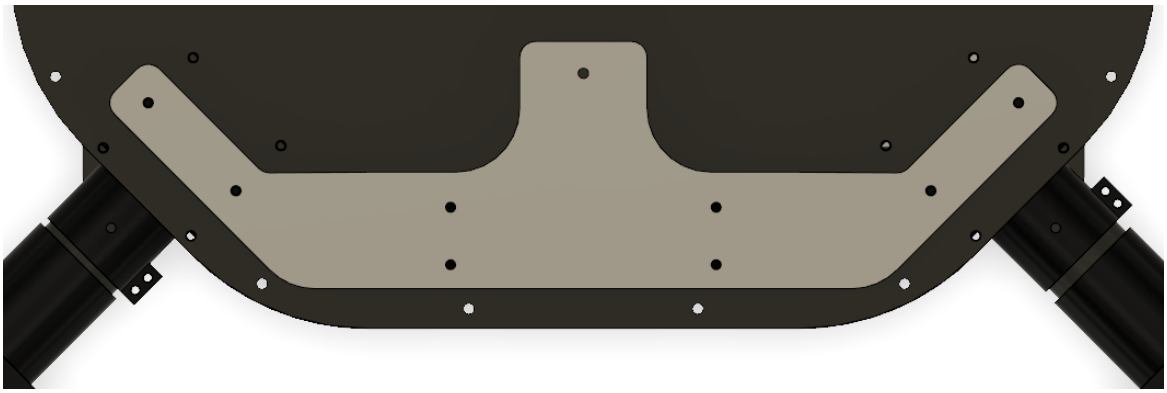

Figure 12. The CAD drawing of the mounting bracket modeled on the top plate of the UAV, without the arm reaching out to the telescope.

The dummy payload was designed to mimic the proper weight distribution and airflow disturbance of the final payload. To accomplish simulating the airflow disturbance, the outside of the payload was made to be the same shape as the actual payload design. To simulate the weight, excess metal components were added inside the tube to ensure that the test payload reached a weight that was at the top of the estimate for the final design. By doing this, it was ensured that the final payload would be easier for the drone to lift than the test article. The weight budget for the test payload is shown in Table 2.

Table 2. The weight budget of the test payload.

Test Payload Weight Budget			
Component	Quantity	Unit Weight (mass)	Total Weight (mass)
Mounting Bracket and Tube Clamps	1	1.35 lb (0.6 kg)	1.35 lb (0.6 kg)
Painted 500mm Tube	1	2.65 lb (1.2 kg)	2.65 lb (1.2 kg)
Lead Weight	1	4.4 lb (2.0 kg)	4.4 lb (2.0 kg)
Metal Plates and Mounting Hardware	1	3.4 lb (1.5 kg)	3.4 lb (1.5 kg)
		Total Weight (mass)	11.8 lb (5.3 kg)

As shown in Table 1, the total weight of the test payload was approximately 5.3 kilograms (11.8 pound). This included a 2 kilogram (4.4 pound) lead weight, which brought up the total weight to our desired range.

After prototyping a few components in CAD based on the weight budget, the team created the first assembly of the UAV and payload together, shown in Figure 13.

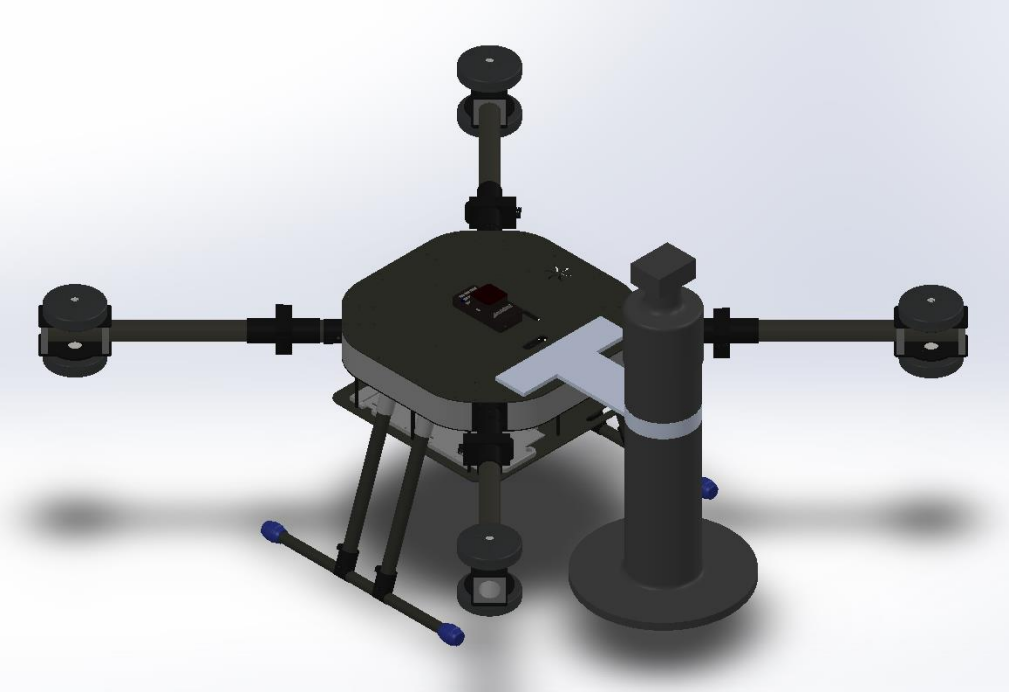

Figure 13. The first mockup of the payload and UAV.

The new payload utilized the same mounting bracket used to mount the main payload to the UAV. There is then an aluminum L-shaped bracket that allows a Canon 80D camera and lens to be mounted. On the opposite side of the L-bracket, battery packs can be stored in a mount manufactured out of Hatchbox PLA filament. Figures 14 show the assembled counterbalance from different angles, and Figure 15 shows the battery packs and their mount.

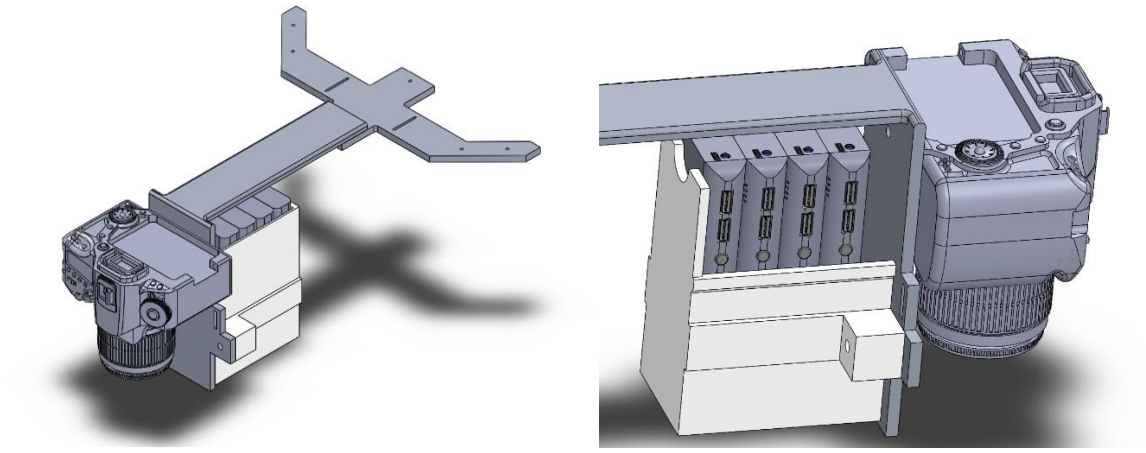

Figure 14. The counterbalance assembly in CAD from a different angles.

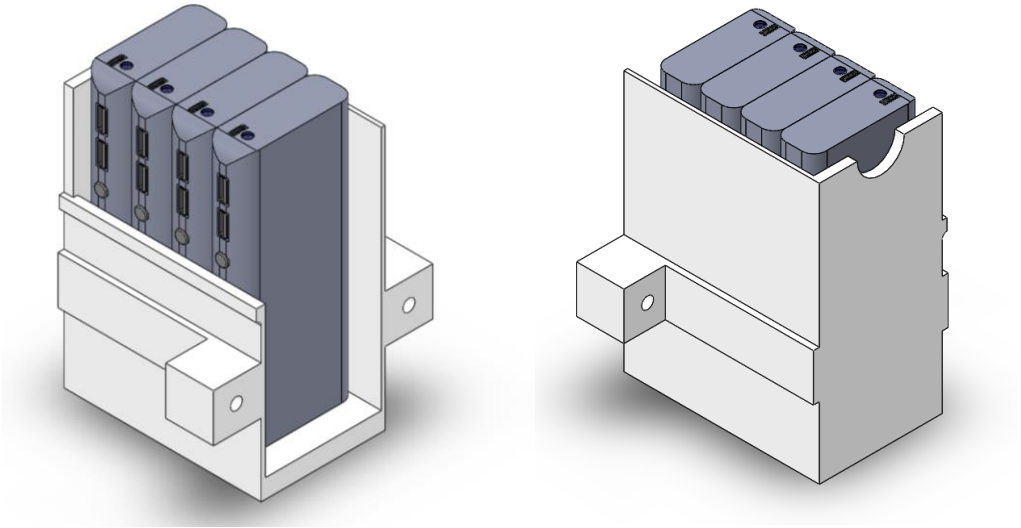

Figure 15. The battery pack mount, oriented to show the accessible USB ports and from the opposite angle.

As can be seen in Figure 15, the battery pack mount was designed to keep the USB ports accessible once mounted. This will allow the batteries to be used to power the lasers on the main payload. Figure 16 shows a photo of the painted “metal plates and mounting hardware” with the tube removed.

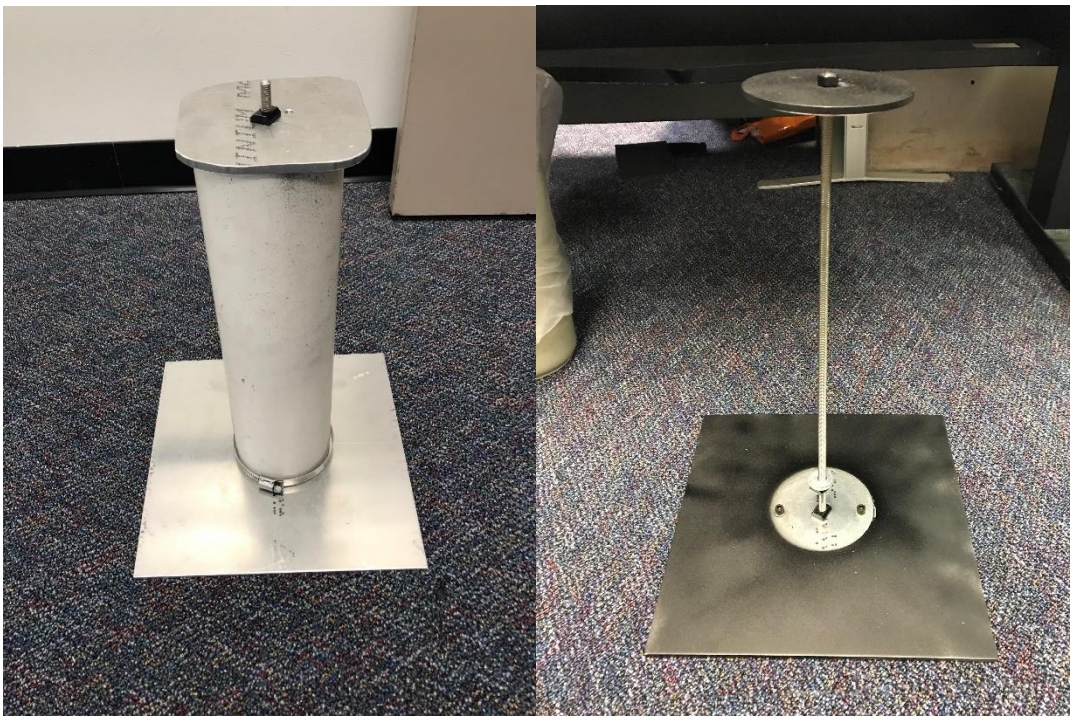

Figure 16. The test payload with and without the tube.

The counterbalance was 4 pounds of zinc stick-on weights mounted to a square carbon fiber tube. The tube was approximately 25.4 mm (1 inch) thick. To compensate for the 5.4 kilogram (12 pound) payload, the weights were positioned approximately 3 times further away from the HIVE x8 body than the center of the payload tube. This distance was determined through testing to position the center of gravity directly under the center of the vehicle's main body. In this position, the carbon fiber tube had holes drilled through it, and zip ties secured the tube to the HIVE x8's auxiliary payload bay, located on the bottom of the UAV. Figure 17 shows a CAD rendering of the counterbalance and the counterbalance on the left side of the HIVE x8 and zip ties and electrical tape to secure the weights.

Figure 17. CAD drawing of the counterbalance (left) and the photo of the counterbalance on payload (right).

After assembly with all the components introduced above, a dummy flight took place in the net outside of Building 1297 at NASA LaRC on July 20, 2018. The payload was prepped and attached to the HIVE-2 vehicle. The vehicle had already been prepped to accept the payload mounting bracket ahead of time. The HIVE-2 was transferred across the center to the net. Figure 18 is the location of the testing site at LaRC.

The approximate net location for flight test is circled in red. During the initial dummy flight testing, Brian Duvall, available at brian.e.duvall@nasa.gov, served as pilot.

Figure 18. The approximate net location for the dummy flight test is circled in red on the map (left) and a photo of the net (right).

The purpose of the dummy test flight in the net was to observe how the HIVE x8 would perform with a payload weight similar or greater to that of a real research flight (Figure 19). The flight was to determine whether the UAV could safely handle such a heavy load. The flight was a simple take off and hover maneuver, and the pilot tested the autopilot's ability to fly on its own. When the UAV demonstrated a pronounced wobble, the pilot attempted to tune the main autopilot board using the controller. After several minutes of flying, the UAV landed.

The flight demonstrated that the HIVE x8 could lift the weight of 5.4 kilogram (12 pound). The weight distribution was determined to be a problem. During the flight test as shown in Figure 20, the UAV developed an oscillation that the autopilot system could not recover from. To an observer, the UAV appeared to rock back and forth in the air between the dummy payload and the counterweight. The pilot was forced to intervene to correct the problem. This would not prove to be a problem under the normal circumstances of a research flight, but could have caused a crash during a real mission if the controller signal was lost. In that situation, the UAV would be forced to rely on its autopilot system to return home and land, and the test demonstrated that this could not be relied on. The oscillation that occurred during the flight was most likely caused by the counterweight. The counterweight was loosely secured with zip ties, and could still move slightly after tightening. The best solution was to develop a custom counterweight that would allow for precise adjustment of the center of gravity.

Figure 19. The photos of the UAV and payload to takeoff for dummy flight test.

Figure 20. A series of photos from the dummy or test flight experiment on July 20, 2018.

Since the UAV demonstration shows that the pilot was capable of flying safely under human control, the next step in the "incremental build-up" approach would be to fly the telescope payload in the net with the revised counterbalance. During this test, the pilot should test to determine if the design changes now allow the autopilot to fly the vehicle on its own. If successful, then more complicated flight maneuvers outside the net could then be attempted.

2.3 Design of the telescope payload

The main device designed for the UAV flight with the PS for image characteristic is the telescope. Figure 21 shows a rendered model of the assembled telescope.

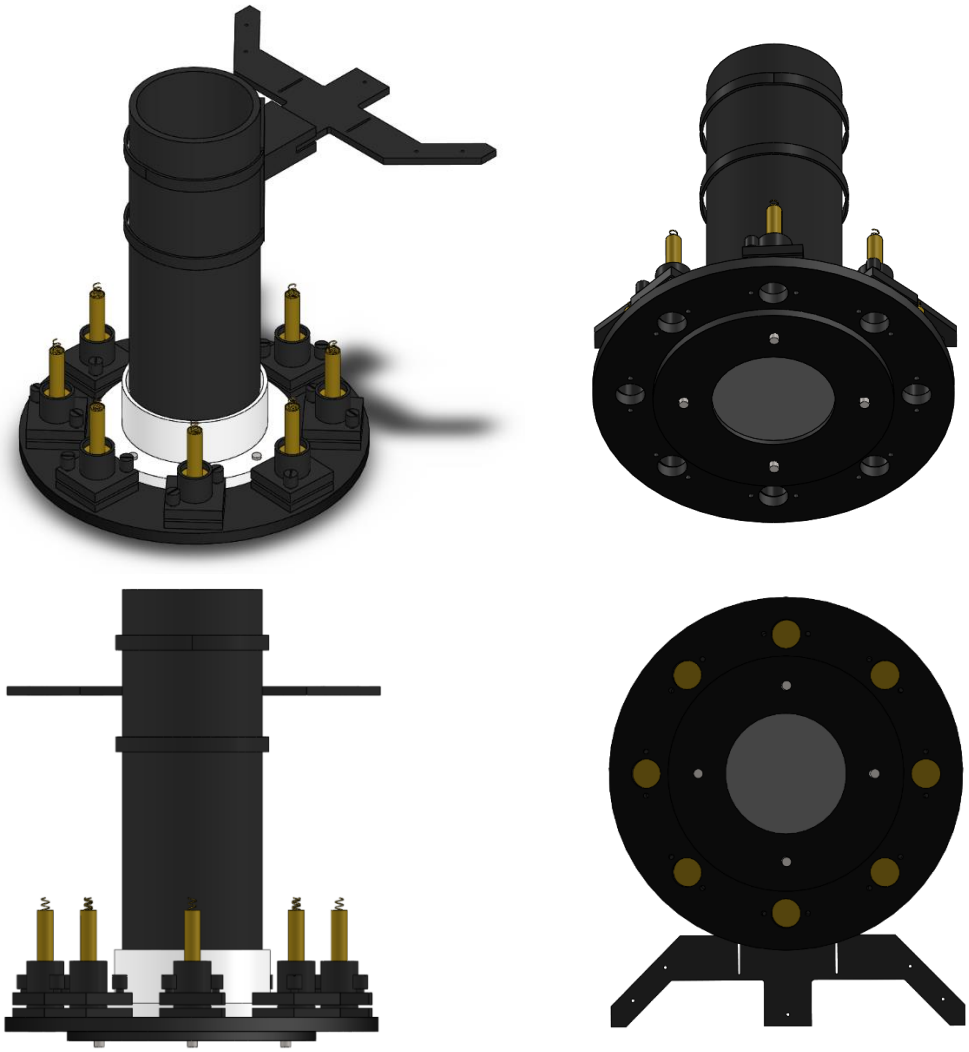

Figure 21. The telescope CAD model.

The component breakdown of this telescope is shown in Figure 22. The telescope can be broken down into three main sections, shown in blue in Figure 22. These sections are the body tube, the lens and laser holder, and the mounting hardware. The components of each of these sections are shown in green.

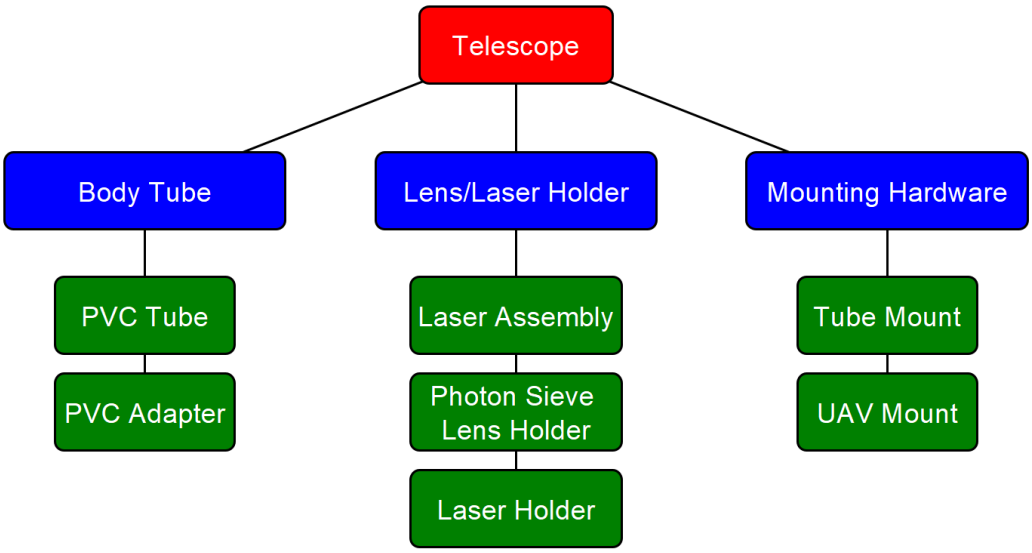

Figure 22. A breakdown of the Photon Sieve Telescope

As can be seen, the mounting hardware contains two components, the tube mount and the UAV mount, as shown in Figure 23.

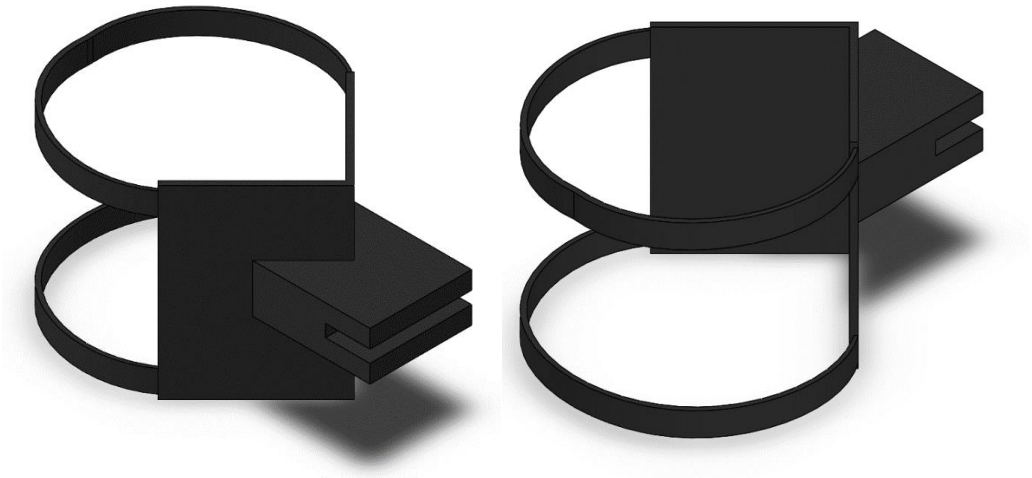

Figure 23. The CAD drawing of the tube mount from two different angles.

This tube mount includes two tube clamps that are tightened around the telescope's main body. The second component, the UAV mount, fits into the slot on the tube mount and is shown in Figure 24 with the dimensions in millimeters. Both the tube mount and the mounting bracket were manufactured using 1060 aluminum alloy. The selected tube clamps are also made out of aluminum. These components have a combined weight of 0.6 kilogram (1.35 pound).

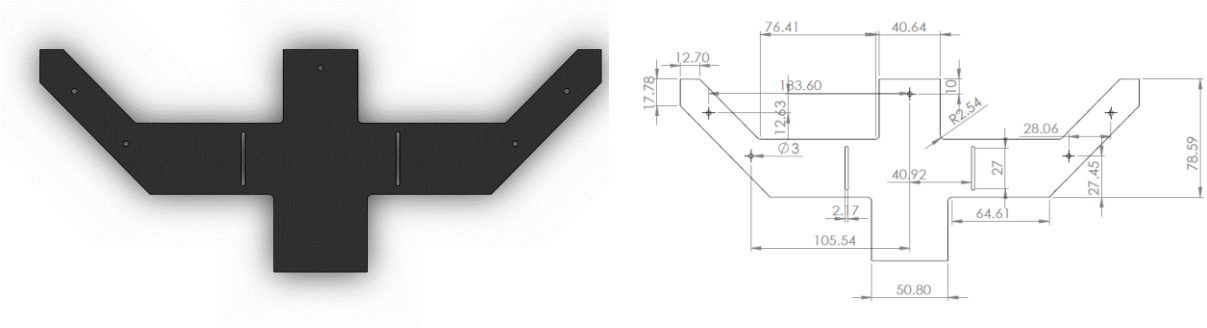

Figure 24. The CAD drawing of the UAV mounting bracket pattern without (left) and with (right) dimensions. Dimensions in diagrams are in millimeters.

The next section of the telescope is the body tube. The body tube, which is shown rendered in Figure 25, is manufactured out of Polyvinyl Chloride (PVC) Schedule 40. This tube has a 101.6-mm (4-inch) inner diameter and has been cut to a length of 450 mm. It weighs approximately 1.2 kilogram (2.65 pound). This body tube serves as the main supporting structure of the telescope. As the center component, both of the other main sections mount to it.

Figure 25. The CAD drawing of the telescope body tube.

The third section of the telescope is the lens and laser holder as shown in Figure 26. This section contains more components than the other two sections combined. To illustrate this, an exploded view of the section is shown.

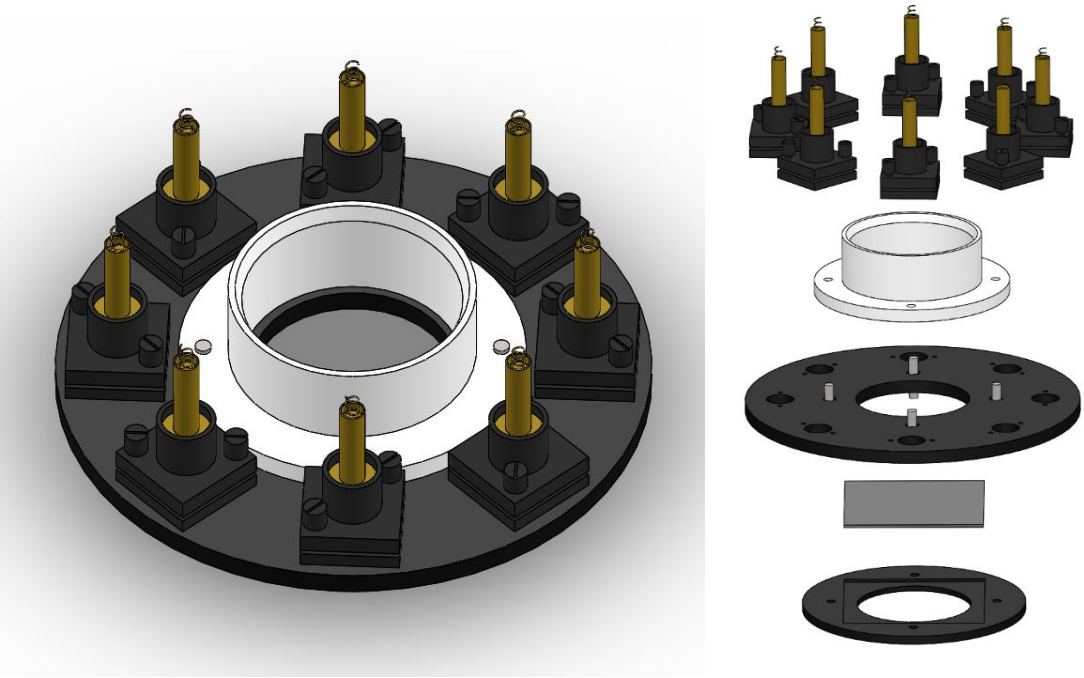

Figure 26. The CAD drawing of the lens and laser holder (left) and an exploded view of the lens and laser holder (right).

Beginning from the top of this exploded view, the first components are eight identical laser assemblies. These assemblies combine a laser with a lens and an adjustable mount. The laser selected is the Quarton Inc. VLM-532-43-SPA, a 5mW, 532nm, continuous wave laser. A close up of one of these laser assemblies is shown in Figure 27. Once mounted to the rest of the lens and laser holder, the two thumbscrews allow for the laser to be focused to a specific spot in front of the telescope. Each of the combined assemblies weigh 181 gram (0.4 pound), meaning that the combined eight weigh 1.45 kilograms (3.2 pounds) in total.

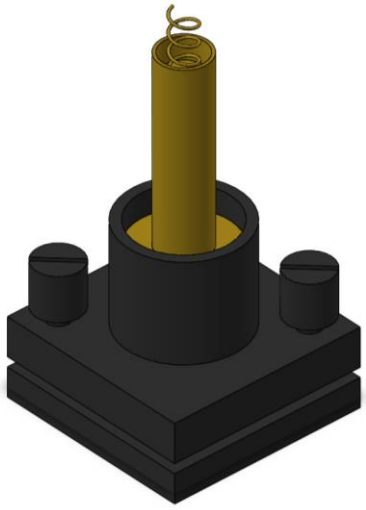

Figure 27. CAD drawing of a single laser assembly.

The next component in the assembly is a standard PVC 101.6 mm (4 inch) tube to drain adapter. This component was selected for its low cost and high strength. It is shown in Figure 28.

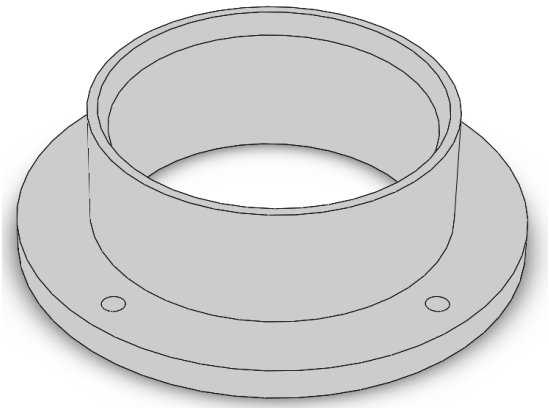

Figure 28. The PVC adapter.

The component mounted under the adapter is the laser mount. This component was designed to support the eight laser assemblies and mounts, as well as serve as the back-plate to the lens. The top side of this component, which mounts to the PVC adapter and the bottom side of this component is shown in Figure 29.

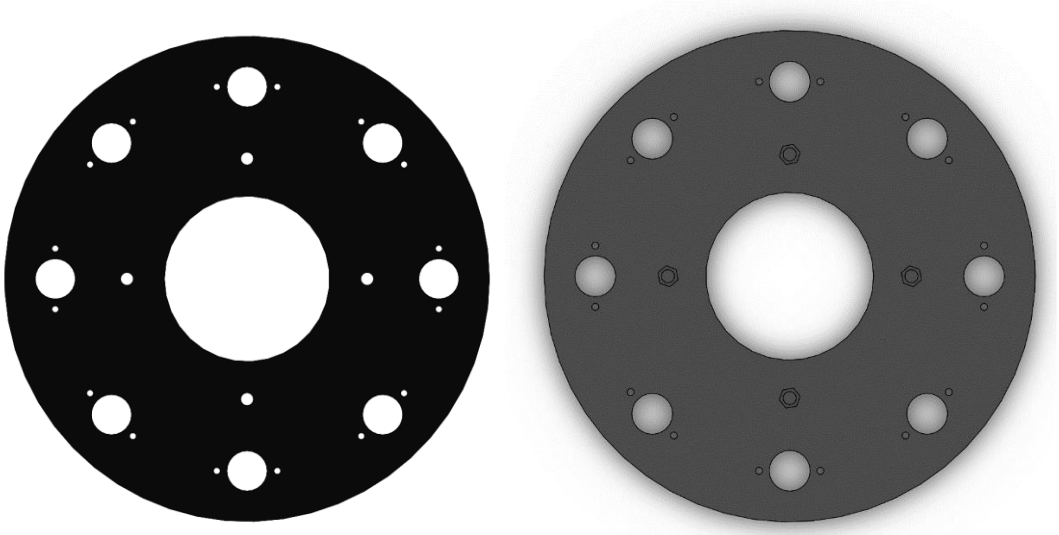

Figure 29. The CAD drawing of the top of the laser mount (left) and the bottom of the laser mount (right)

Of significant note in the design of this holder are the four slots which allow nuts to be embedded into the plastic. This design choice allows the laser holder to remain fixed in place while other components are removed. Due to the comparatively frequent removal of the other pieces, this design could save time. Dimensions of the slots and other components are shown in Figures 30. This component was manufactured out of Gigabot Black PLA filament using the NASA LaRC Makerspace's Gigabot XL 3+ printer. The final product weight of the component after the print was 0.85 pounds.

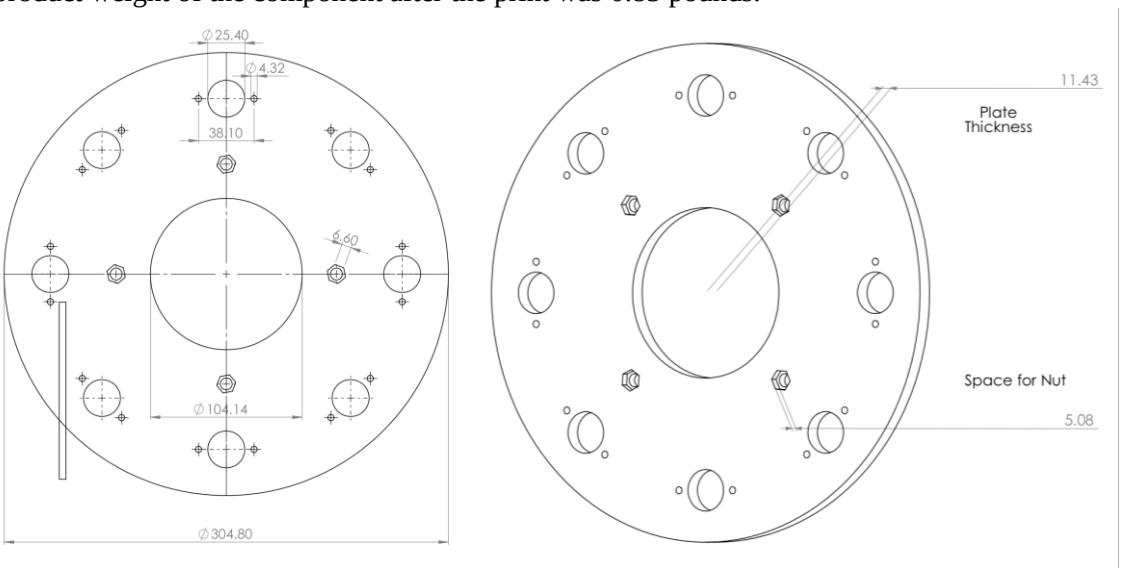

Figure 30. CAD drawing of the bottom of the laser holder with dimensions. Dimensions in diagrams are in millimeter.

The last component for the telescope payload is the lens holder, which was designed to be quickly attached and detached using four nuts. The rendered drawing with dimensions is shown in Figure 31. This lens holder was manufactured using Hatchbox Black PLA filament. When completed, it weighs approximately 181 gram (0.4 pound) and has a thickness of 6 mm (0.24 inch). The square cut has 2.3 mm (0.09 inch) depth.

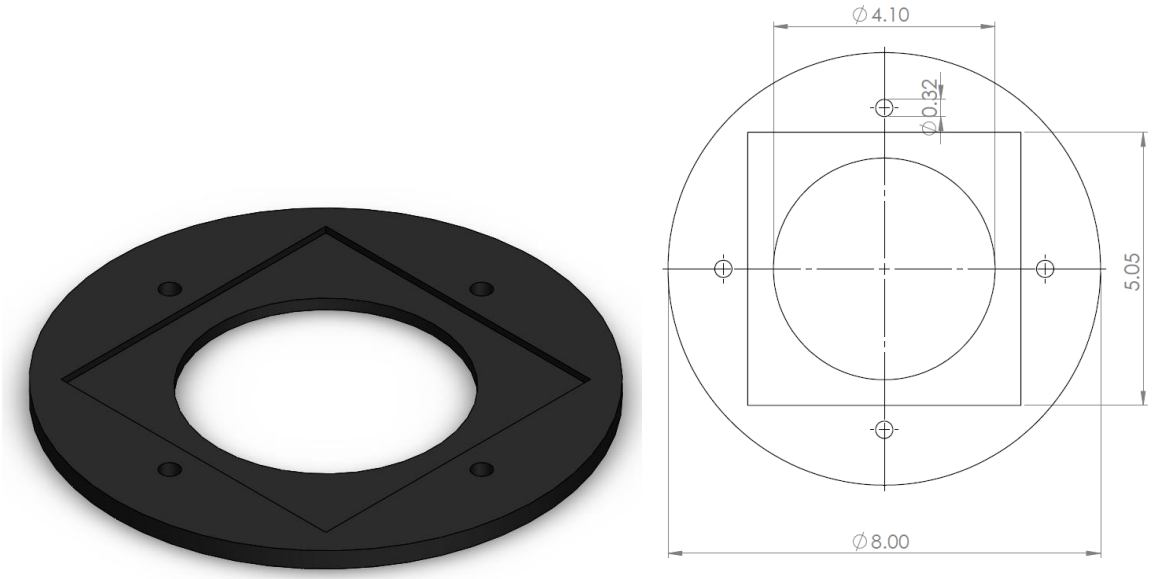

Figure 31. CAD drawing of the lens holder, commonly called the photon sieve holder with and without dimensions. Dimensions are in inches (Multiple the length value by 25.4 for millimeter dimension).

All of these components combine to give the payload a total weight of 9.85 pounds. A breakdown of this weight budget is provided in Table 3.

Table 3. The weight budget for the telescope payload (lb. is a pound by weight).

Photon Sieve Telescope Weight Budget			
Component	Quantity	Unit Weight (lb)	Combined Weight (lb)
Mounting Bracket	1	1.35	1.35
Tube (painted)	1	2.65	2.65
Laser Diode Assembly	8	0.2	1.6
Laser Mount	8	0.2	1.6
Camera Adapter	1	0.5	0.5
Tube->PS Holder Adapter	1	0.65	0.65
PLA Laser Plate	1	0.85	0.85
Photon Sieve Holder	1	0.4	0.4
Mounting Hardware	1	0.25	0.25
Photon Sieve	1	0.3	0.3
GoPro	1	0.25	0.25
		Total Weight (lb):	10.4
		Total Mass (kg):	4.72

2.4 Camera selections

Proper camera selection and optimization of the camera setting to take high-quality data through the photon sieve is important. Following are the requirements for the camera.

- The camera should be disposable / less expensive or have a more robust control system.
- To prevent motion blurring at approximately 56 kilometer per hour (kph, 35 miles per hour), the shutter speeds should be faster than 100 milliseconds.
- Maximum shutter opening time for the lower framerate is required. After the longest shutter speed is obtained, the highest resolution should be selected.

Both Canon EOS 80D and GoPro cameras and three other cameras (a FDR-X3000, a Basler ace acA2500-14gm, and a IDT NX4 Air) were evaluated for the telescope payload test. The pros and cons of each camera are discussed and a summary of important notes for each of the test cameras are documented in Table 4.

Table 4. A comparison of the five cameras.

Current and Future Photon Sieve Telescope Camera Comparison					
Description	GoPro	Sony Action Camera	Machine Vision Cameras	Professional Slo-Mo Scientific Camera	DSLS
Manufacturer	GoPro	Sony	Basler	IDT	Canon
Model Number	HERO6	FDR-X3000	Ace acA2500-14gm	NX4 Air	80D
Approximate Price	$500	$360	$500	$30,000	$1,000
Max. Resolution	4096 × 3072	4608 × 2592	2592 × 1944	1024 × 1024	6000 × 4000
Max. Framerate	240fps at 1080p, 60fps at 4000p	240fps at 720p, 30fps at 4000p	14fps	3000fps	50fps at 1080
Control Method	Touch Screen, Wireless from Phone	Built in buttons, Wireless	Ethernet wire to computer, LabView code	Wired or Wireless control from computer	Manual: Wireless over Wi-Fi link
Control Software	GoPro Phone App	Sony Remote Control	Custom LabView Vision Development Module Code ($6,000 license)	IDT motion studio (included with purchase)	EOS Utility
Data Transfer Method	Removable MicroSD	Removable MicroSD	Stored on connected computer	Onboard storage, wired or wireless data transfer to computer	Removable SD card, wireless data transfer
Sensor Size	6.17mm×4.63mm	7.2mm×7.2mm	5.7mm×4.3mm	13.9mm×13.9mm	22.5mm × 15.0mm
Pixel Size	1.6µm×1.6µm	N/A	2.2µm×2.2µm	13.68µm×13.68µm	3.72µm × 3.72 µm
Image Color	Yes	Yes	No, B/W	Yes	Yes

- GoPro HERO6 – The GoPro is a smart action camera that is capable of high resolution and framerates (4k/60fps or 1080p/240fps). The version owned by the PS Team has been modified to accept C-mount lenses. The GoPro is sturdy, versatile, and features a removable battery that can be swapped between drone flights. Its restrictions include its sensor size and its limited amount of control. The GoPro does not accept wired control, and functions as an independent unit unless a smartphone is connected [20].
- Sony FDR-X3000 – The Sony is an action camera intended to compete with the GoPro. It's main benefits include its price ($400 to $550), its sturdy build quality (waterproof and designed for impacts), and its size. However, its settings menu is even more restrictive than the GoPro, and the sensor/pixel size is tiny. Additionally, this is the only camera of the four that cannot be purchased with a C-mount adapter. This camera, like the GoPro, can function independently and does not need a controlling computer or code to run [21].

- Basler ace acA2500-14gm – The Basler is a machine vision camera that is powered and controlled by an Ethernet port. It is the smallest of the three cameras. It is limited to 14fps, but all standard camera settings can be controlling LabView code. The camera needs the Labview Vision Development Module (cost: $6,000) to run, and it must remain attached to the host computer. No independent or wireless option is available [22].
- IDT NX4 Air – The IDT is a professional slow motion camera. It is large and heavy compared to the other cameras in Table 4, but offers the most control of its settings. The camera is controlled by a host computer running software that is included with the camera, and a wireless module is available to control the camera from afar. The camera saves video to onboard storage, and can achieve a framerate of 3000fps. This comes with a caveat of using large amounts of storage space. The camera can only record at 1000fps for 6 seconds before the data must be offloaded [23].
- Canon EOS 80D – The Canon is a consumer-grade DSLR camera. It allows many of its settings to be manually controlled, but does not have an established method for pre-programming a control sequence. Remote operation is possible by the use of Canon's EOS Utility software, which connects a windows computer to the camera through a Wi-Fi link. The Canon can take the highest resolution images of any of the five cameras, with a max resolution of 6000x4000, but its maximum video resolution is limited to 1080p. In video mode, the Canon is capped at 60fps [24].

Figure 32. Photos of candidate cameras for the telescope payload. Left to right shows GoPro HERO6, Basler acA2500-14gm, Sony FDR-X3000, IDT NX4 Air, and Canon EOS 80D

3. Summary

The Photon Sieve (PS) team at NASA Langley Research Center (LaRC) began receiving support for the development and characterization of PS devices through the NASA Internal Research & Development Program (IRAD) in 2015. The project involves ascertaining the imaging characteristics of various PS devices. The next goal of the project is to design and develop a telescope and image capture system as a drone-based payload instrument.

The photon sieve essentially acts as a lens to diffract light to a concentrated point on the focal plane. In the fields of astronomy, remote sensing, and other applications that require imaging of distant objects both on the ground and in the sky, it is often necessary to perform post-process filtering in order to separate noise signals that arise from multiple scattering events near the collection optic. The PS shows a novel filtering technique by avoiding the unwanted signal without time consuming post process for imaging application. Furthermore, it offers a promising solution for high resolution imaging with suppressed side-lobes than the Fresnel Zone Plate (FZP). The PS holds the potential to significantly reduce mission costs and improve imaging quality by replacing traditional reflector telescopes.

This project used Langley resources to design, manufacture, and characterize a series of photon sieve samples. After a prototype was developed and characterized in the laboratory, outside testing was conducted to obtain moon images by using a telescopic setup. The 152.4 mm (6 inch) diameters design was manufactured on Cr-coated soda lime glass substrate for imaging test. The USAF target produces a sharp image that .89 lines per mm is clearly resolvable by using the PS. Furthermore, the moon image quality taken from the PS is comparable with the image taken by 1.5 meter (5 feet) diameter of telescope from Consolidated Lunar Atlas. For a drone-based image capture system, the PS team selected UAV and camera, evaluated a weight budget of each components, designed telescope, and completed a flight safety review / approval process from the LaRC Airworthiness Safety Review Board (ASRB). The preliminary test was conducted by using a NASA hive model 1200 XE-8 research Unmanned Aerial Vehicle and dummy payload.

4. Future work

The next version of the telescope structure will be designed around diffractive optics components and commercially available camera electronics to create a lightweight payload for ocean surface imaging, as shown in Figure 33. The new PS telescope on the drone will use a range detecting optics system for exploration science. Additional future work for the project includes designing a near-field PS, assembling a telescope system with a PS, camera, and lasers, and conducting a drone-based flight test by using the telescope assembly.

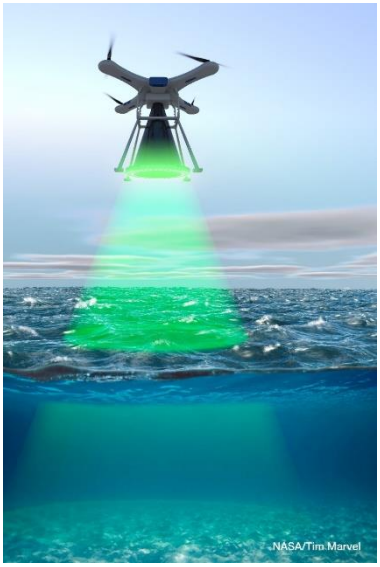

Figure 33. Concept drawing of the ‘range detecting diffractive optics imaging system’ (drawn by Tim Marvel, graphic designer at NASA LaRC, NASA LaRC PS team credit).

Following is the main tasks for the future project.

(1) A new design of a PS for near-field focusing:
Traditionally the PS requires a planar wavefront (i.e., infinite distance object such as the moon) to properly focus light. By modifying the PS design equation to account for wavefront curvature, PS’s will be designed to focus light from objects at near-field distances (such as the ocean surface viewed from the drone). The near-field PS design eliminates the requirement of an infinite Radius of Curvature (RoC) wavefront and

allowing for imaging of objects very near the optics. Finally, the modified PS design would be for 'near-field' focusing and 'infinite-field' filtering. In order to achieve this, it is a simple matter of using geometry to alter the position of photon sieve rings to account for the phase delay of light between the center of the sieve (which would arrive first in a spherical wavefront) and the edge of the sieve (which would arrive later than the center). Additionally, the sizes of the pinholes are re-adjusted to account for their new radial position.

(2) Manufacture the new PS on Cr-coated soda lime glass substrate to proof the math of the near-field PS design.

(3) Develop flexible substrate for light-weight PS and potential space applications:
In addition to the future PS project, new polymer development research will be conducted in the cleanroom as next generation space optical lenses. The flexible films would be polyimide, SiO_2 coated Mylar, and cellulose NanoFiber (CNF). However, there is no limitation on the selection of the type of film as long as the material exhibits the proper merits of light-weight, high-transparency, high thermal-stability, low-outgassing, and radiation resistance. Under this effort, the MISSE-12 (Materials International Space Station Experiment) flight facility experiment was selected as the testbed with an approximate launch date of September 2019.

(4) Drone setup for ocean surface imaging
The final step of the future work is to design and develop a telescope and image capture system by using a drone-based payload instrument. For the flight test, a NASA hive model 1200 XE-8 research Unmanned Aerial Vehicle (UAV, 9 kg maximum payload, 25 minutes flight time), near-field PS, laser assembly, and a GoPro camera will be assembled and tested.

5. Acknowledgement

The work in this technical memorandum was supported by an Internal Research & Development Program (IRAD) award at NASA Langley Research Center.

The authors appreciate the support and assistance of the NASA LaRC photon sieve team (Wenbo Sun, Yongxiang Hu, Matthew Julian, Ken Tedjojuwono, Brian Walsh, Shawn Britton, John Leckey) and NIFS students (Grant Gibson from the University of Virginia, Sean Fitzpatrick from the Georgia Institute of Technology, Shravan Hariharan from the Georgia Institute of Technology, Benjamin Bogner from Benedictine College, Ethan Gorham from the University of Central Florida, and Risa Purow-Ruderman from Charlottesville High School).

The authors also thank Thomas Jones, William Humphreys, and Edward Adcock at AMDSB, the ASRB committee (Brent Weathered as the Chair, Brian Beaton from UASOO, and Vanessa Aubuchon as the Technical Secretary), Brian Duvall (drone pilot), Danette Allen (LaRC Autonomy Incubator), and Dan Healy (flight test coordinator) for their help, fruitful discussion, and support during the work.

6. References

1. L. Kipp and M. Skibowski, R. L. Johnson, R. Berndt, R. Adelung, S. Harm and R. Seemann, Sharper images by focusing soft X-ray with photon sieves, Nature 414 (2001) 184–188.

2. J. M. Davila, High-resolution solar imaging with a photon sieve, Proc. SPIE 8148, Solar Physics and Space Weather Instrumentation IV, 81480O (6 October 2011); doi: 10.1117/12.898956.
3. Q. Cao and J. Jahns, Nonparaxial model for the focusing of high-numerical-aperture photon sieves, J. Opt. Soc. Am. A20 (2003), 1005–1012.
4. Q. Cao and J. Jahns, Focusing analysis of the pinhole photon sieve: individual far-field model, J. Opt. Soc. Am. A19 (2002), 2387–2393.
5. R. Liu, F. Li, M. J. Padgett, and D. B. Phillips, Generalized photon sieves: fine control of complex fields with simple pinhole arrays, Optica 2 (2015), 1028-1036.
6. S. Park, B. Park, S. Nam, S. Yun, S. K. Park, S. Mun, J. M. Lim, Y. Ryu, S. H. Song, and K.U. Kyung, Electrically tunable binary phase Fresnel lens based on a dielectric elastomer actuator, Opt. Express 25 (2017), 23801-23808.
7. W. Sun, G. Videen, S. Kato, B. Lin, C. Lukashin, and Y. Hu, A study of subvisual clouds and their radiation effect with a synergy of CERES, MODIS, CALIPSO and AIRS data, J. Geophys. Res. 116(D22) (2011), D2207.
8. W. Sun, G. Videen, and M. I. Mishchenko, Detecting super-thin clouds with polarized sunlight, Geophys. Res. Lett. 41(2) (2014), 688–693.
9. W. Sun, R. R. Baize, G. Videen, Y. Hu, and Q. Fu, A method to retrieve super-thin cloud optical depth over ocean background with polarized sunlight, Atmos. Chem. Phys. 15(20) (2015), 11909–11918.
10. W. Sun, Y. Hu, D. G. MacDonnell, C. Weimer, and R. R. Baize, Technique to separate lidar signal and sunlight, Opt. Express 24(12) (2016), 12949–12954.
11. G. Andersen, Large optical photon sieve, Opt. Lett. 30 (2005), 2976-2978.
12. G. Andersen and D. Tullson, Broadband antihole photon sieve telescope, Appl. Opt. 46 (2007), 3706-3708.
13. S. Hariharan, S. Fitzpatrick, M. Julian, H. J. Kim, and D. Macdonnell, Rapid generation of large dimension phonon sieve designs, NASA/TM-2017.
14. H. J. Kim and T. Jones, Active optic component development: unique capabilities within the Advanced Measurement and Data Systems Branch at NASA LaRC, NASA Technical Interchange Meeting on Active Optical Systems for Supporting Science, Exploration, and Aeronautics Measurements Needs, NASA-TM, 2018.
15. A. F. Chrimes, I. Khodasevych, A. Mitchell, G. Rosengarten, and K. Kalantar-zadeh, Dielectrophoretically controlled Fresnel zone plate, Lab on a Chip 15 (2015), 1092-1100.
16. J. Ke and J. Zhang, Generalized Fibonacci photon sieves, Appl. Opt. 54 (2015), 7278-7283.
17. A. Sabatyan and S. Mirzaie, Efficiency-enhanced photon sieve using Gaussian/overlapping distribution of pinholes, Appl. Opt. 50 (2011), 1517-1522.
18. M. N. Julian, D. G. MacDonnell, and M. C. Gupta, High efficiency flexible multilevel photon sieves by single-step laser-based fabrication and optical analysis, Applied Optics 58 (1) (2019), 109-114.
19. ISO 14644-1: Cleanrooms and associated controlled environments - Part 1: Classification of air cleanliness by particle concentration (2015).
20. https://shop.gopro.com/cameras/hero6-black/CHDHX-601-master.html
21. https://www.sony.com/electronics/actioncam/fdr-x3000-body-kit#product_details_default
22. https://www.baslerweb.com/en/products/cameras/area-scan-cameras/ace/aca2500-14gm/#tab=specs
23. https://idtvision.com/products/cameras/nx-series-cameras/
24. https://www.usa.canon.com/internet/portal/us/home/support/details/cameras/dslr/eos-80d?tab=technicalspecifications

REPORT DOCUMENTATION PAGE

Form Approved
OMB No. 0704-0188

1. REPORT DATE *(DD-MM-YYYY)*
1-02-2019

2. REPORT TYPE
Technical Memorandum

3. DATES COVERED *(From - To)*

4. TITLE AND SUBTITLE
Photon Sieve Design and Fabrication for Imaging Characteristics using UAV Flight

5a. CONTRACT NUMBER

5b. GRANT NUMBER

5c. PROGRAM ELEMENT NUMBER

6. AUTHOR(S)
Kim, Kyun-Jung; Aguillard, John; Julian, Mathew; Bartram, Scott; Macdonnell, David G.

5d. PROJECT NUMBER

5e. TASK NUMBER

5f. WORK UNIT NUMBER
432938.09.01.07.05.05

7. PERFORMING ORGANIZATION NAME(S) AND ADDRESS(ES)
NASA Langley Research Center
Hampton, VA 23681-2199

8. PERFORMING ORGANIZATION REPORT NUMBER
L-20999

9. SPONSORING/MONITORING AGENCY NAME(S) AND ADDRESS(ES)
National Aeronautics and Space Administration
Washington, DC 20546-0001

10. SPONSOR/MONITOR'S ACRONYM(S)
NASA

11. SPONSOR/MONITOR'S REPORT NUMBER(S)
NASA-TM-2019-220252

12. DISTRIBUTION/AVAILABILITY STATEMENT
Unclassified-
Subject Category 27
Availability: NASA STI Program (757) 864-9658

13. SUPPLEMENTARY NOTES

14. ABSTRACT
The Photon Sieve (PS) team at NASA Langley Research Center (LaRC) began receiving support for the development and characterization of PS devices through the NASA Internal Research & Development Program (IRAD) in 2015. The project involves ascertaining the imaging characteristics of various PS devices. These devices hold the potential to significantly reduce mission costs and improve imaging quality by replacing traditional reflector telescopes. The photon sieve essentially acts as a lens to diffract light to a concentrated point on the focal plane like a Fresnel Zone Plate (FZP). PS's have the potential to focus light to a very small spot which is not limited by the width of the outermost zone as for the FZP and offers a promising solution for high resolution imaging. In the fields of astronomy, remote sensing, and other applications that require imaging of distant objects both on the ground and in the sky, it is often necessary to perform post-process filtering in order to separate noise signals that arise from multiple scattering events near the collection optic. The PS exhibits a novel filtering technique that rejects the unwanted noise without the need for time consuming post processing of the images.

15. SUBJECT TERMS
Imaging; Optics; Photon sieve; Telescopes; UAV

16. SECURITY CLASSIFICATION OF:			17. LIMITATION OF ABSTRACT	18. NUMBER OF PAGES	19a. NAME OF RESPONSIBLE PERSON
a. REPORT	b. ABSTRACT	c. THIS PAGE			STI Help Desk (email: help@sti.nasa.gov)
U	U	U	UU	38	19b. TELEPHONE NUMBER *(Include area code)* (757) 864-9658